Meccanica (2015) 50:2663–2673
DOI 10.1007/s11012-015-0164-6

SOFT MECHATRONICS

Humidity-dependence of IPMC sensing dynamics: characterization and modeling from a physical perspective

Hong Lei · Chaiyong Lim · Xiaobo Tan

Received: 18 September 2014 / Accepted: 20 March 2015 / Published online: 1 April 2015

Abstract Ionic polymer−metal composites (IPMCs) exhibit humidity-dependent sensing behavior when operating in air, which weakens the reliability of the IPMC sensors. To better understand the underlying physics of this behavior and capture the humidity-dependence analytically, in this paper the influence of the ambient humidity on IPMC sensors is characterized and modeled from a physical perspective. In particular, we study a cantilevered IPMC beam subjected to base-excitation inside a custom-built humidity chamber with controlled humidity level. The empirical frequency responses of the sensor dynamics under different humidity levels are first obtained. Charging experiments are also conducted under each humidity level, in order to identify the corresponding effective dielectric constant. At each given humidity level, the humidity-dependent physical parameters are identified by curve-fitting the measured frequency responses with the model predictions. These identified parameters indicate a noticeable dependence on the humidity, which is captured with polynomial functions. The polynomial functions are then plugged into the physics-based model to predict the sensing output of the IPMC sensor under other humidity conditions. Additional experimental results are presented to support the effectiveness of the model.

Keywords Ionic polymer−metal composite · Humidity · IPMC sensing · Modeling · Electroactive polymer

H. Lei (✉) · X. Tan
Smart Microsystems Laboratory, Department of Electrical and Computer Engineering, Michigan State University, East Lansing, MI 48824, USA
e-mail: leihongbuaa@gmail.com

X. Tan
e-mail: xbtan@egr.msu.edu

C. Lim
Department of Electrical Engineering, Arizona State University, Tempe, AZ 85287, USA
e-mail: Chaiyong.Lim@asu.edu

1 Introduction

Ionic polymer−metal composites (IPMCs), one important class of electroactive polymers (EAPs), have been studied extensively for the past decade [1, 2]. With built-in sensing and actuation capabilities, IPMCs hold strong promise for applications in a number of engineering areas. As actuators, they require low driving voltages (<3 V) to generate large bending deformation; as sensors, they have inherent polarity, capability of working in both air and water, and direct mechanosensory property, which minimizes the structural complexity for both sensor construction and signal processing. An IPMC sample typically consists of one layer of ionomeric membrane (typically Nafion) and two layers of electrodes (typically noble metal, e.g. platinum), which are

formed by chemical deposition on both surfaces of the membrane. Inside the polymer membrane, anions of negative charges are fixed to the polymer chains while cations of positive charges are hydrated and can move freely. When the IPMC is subjected to a mechanical deformation, the redistribution of the cations and accompanying solvent molecules inside the polymer will generate a detectable electrical signal across the electrodes, which can be open-circuit voltage or short-circuit current. This charge redistribution explains the sensing mechanism of IPMCs. Recent years tremendous effort has been made in the fabrication [3–9], characterization [10–18] and modeling [19–24] of IPMC actuators and sensors. Potential applications of IPMC sensors are also explored for the measurement of force [25], curvature [26], flow [27] and shear loading [28], structural health monitoring [29], and energy harvesting [30–33].

A critical issue for IPMC sensors is that they need ionic hydration to operate in air. As the most commonly used solvent in IPMCs, water content varies with the humidity level of the ambient environment, leading to the inconsistent sensing behavior of an IPMC in air. Therefore, it is of importance to study the humidity-dependent sensing behavior of IPMCs. Some work has been reported on characterizing the influence of humidity on IPMCs. Bauer et al. [10] studied the humidity influence on the mechanical properties of a Nafion 117 membrane. Shoji and Hirayama [11] characterized the humidity influence on the IPMC actuators experimentally. Brunetto et al. [12, 13] used a linear model to characterize the humidity effect on IPMC sensing properties by statistically studying the sensing signals under typical working conditions. Park [16] investigated the solvent evaporation effect on IPMC sensors based on a circuit model and found the optimum hydration level for a surface-mounted sensor. On a related note, linear empirical models have been proposed to capture the temperature-dependence of IPMC sensors [14] and actuators [15].

In this paper, in order to understand the underlying physics of this humidity-dependence and minimize its influence, we characterize and model the effect of environmental humidity on IPMC sensors from a physical perspective. Specifically, we present a dynamic physical model for a cantilevered IPMC beam that is excited mechanically at its base inside a custom-built humidity chamber, where the humidity is feedback-controlled by activating/deactivating a humidifier or a dehumidifier properly. We first measure the frequency responses of the sensor under different humidity levels, with the IPMC base displacement as input and the tip displacement and short-circuit current as outputs. Constant-voltage charging experiments of the IPMC are also conducted under each humidity level. At each given humidity level, we then curve-fit the empirical frequency responses with the prediction of the physics-based model to identify the humidity-dependent physical parameters, including Young's modulus, strain-rate damping coefficient, and viscous air damping coefficient for the mechanical properties, and ionic diffusivity for the mechanoelectrical dynamics. Data from the charging experiments are directly used to estimate the effective dielectric constant. These parameters show a clear trend of changing with the humidity. By fitting the identified parameters at a set of test humidity levels, the humidity-dependence of the physical parameters is captured with polynomial functions, which are then plugged into the physics-based model for IPMC sensors to predict the sensing output under other humidity conditions. The latter humidity-dependent model is further validated with experiments, indicating the potential that we can obtain more accurate IPMC sensor measurements in real-world applications if the humidity level information is available.

A preliminary version of some results was presented at a conference [34]. The current paper represents significant enhancements over [34], including an improved dynamic model incorporating the air damping term, separate charging experiments to study the influence of humidity on dielectric constant, new experimental approach to minimize the gravity effect and reduce the humidity variation during the data-collection period, and consideration of the change of the thickness and the mass per unit length under different RH levels.

The remainder of the paper is organized as follows. A dynamic, physics-based model for a base-excited IPMC sensor is first reviewed in Sect. 2. The experimental setup and parameter identification process are described in Sect. 3. The identified humidity-dependent model and its validation results are presented in Sect. 4. Finally, concluding remarks are provided in Sect. 5.

2 Review of a dynamic model for an IPMC sensor under base excitation

In this study, we characterize and model the humidity influence on IPMCs based on a dynamic, physical model which describes a base-excited IPMC sensor in the form of a cantilevered beam [35]. The configuration of base excitation finds potential applications in energy harvesting and structural monitoring [29, 36], and is convenient for implementation in experiments within a relatively large frequency range. The reviewed model has a closed-form expression, and combines the vibration dynamics of a base-excited flexible beam and the ion transport dynamics within the IPMC. Euler–Bernoulli cantilever beam theory is used to describe the mechanical vibration of the IPMC, which incorporates strain-rate damping and viscous air damping. The governing PDE in [37] is adopted to model the ion transport dynamics, which accounts for electrostatic interactions, ionic diffusion and ionic migration along the beam thickness direction. Expressed in terms of sensor dimensions and fundamental physical parameters, this model for base-excited IPMC sensors takes the form of a transfer function and relates the sensing signal (short-circuit current) to the mechanical base vibration, which enables us to study the humidity dependence of the physical parameters based on the experimental observations.

Figure 1 shows the configuration of a base-excited IPMC, where the beam, clamped at one end ($z = 0$), is subjected to a base vibration $u(t)$, generating the bending displacement $w(z,t)$ along the length direction and a short-circuit sensing current $i(t)$. The neutral axis of the beam is denoted by $x = 0$, and the two surfaces are denoted by $x = h$ and $x = -h$, respectively. The $y-z$ plane is parallel to the beam plane when the beam is not deformed. Unlike the configuration in [29, 34], where the beam was excited up and down, in this study the IPMC vibrates within the horizontal plane, which is parallel to the $x-z$ plane. By placing the IPMC in this way, the gravity effect of the beam mass can be ignored. Assume that the IPMC undergoes small deformation during the vibration, and that the IPMC beam has a considerably smaller thickness $2h$ than its length L and width b. Then the beam displacement $w(z,t)$ can be described

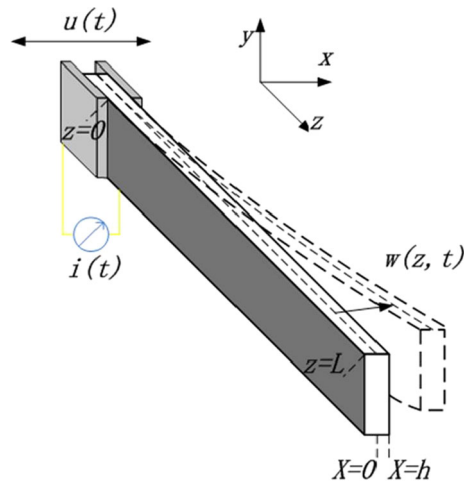

Fig. 1 Geometric definition of an IPMC beam subjected to base excitation (*top-view*)

by the following Euler–Bernoulli beam equation with strain-rate (or Kelvin–Voigt) damping and viscous air damping [38, 39]:

$$YI\frac{\partial^4 w(z,t)}{\partial z^4} + C_s I\frac{\partial^5 w(z,t)}{\partial z^4 \partial t} + C_a\frac{\partial w(z,t)}{\partial t} + m\frac{\partial^2 w(z,t)}{\partial t^2} = 0, \tag{1}$$

where Y denotes the Young's modulus, $I = \frac{2}{3}bh^3$ is the moment of inertia of the beam cross-section, m is the mass per unit length of the beam, and C_s and C_a are the strain-rate damping coefficient and viscous air damping coefficient, respectively. It is a simple approach to use viscous air damping to model the force of air particles that acts on the beam during the vibration. The composite structure of the IPMC is assumed to demonstrate linear-viscoelastic material behavior, hence the strain-rate damping is included in (1), accounting for the structural damping due to the internal energy dissipation of the beam. The transformed displacement $W(z,s)$ is then given by the following equation in the Laplace domain [29]:

$$W(z,s) = U(s)\frac{N_1(z,s)}{D_1(s)}, \tag{2}$$

where

$$
\begin{aligned}
D_1(s) &= \cosh^2(pL) + \cos^2(pL),\\
N_1(z,s) &= D_1(s)\cos(pz)\cosh(pz)\\
&\quad + C_2(s)(\sin(pz)\cosh(pz)\\
&\quad - \cos(pz)\sinh(pz))\\
&\quad - C_3(s)\sin(pz)\sinh(pz),\\
C_2(s) &= \cos(pL)\sin(pL) + \cosh(pL)\sinh(pL),\\
C_3(s) &= \cosh^2(pL) - \cos^2(pL),\\
p &= k\sqrt{s},\\
k &= \sqrt[4]{\frac{C_a + ms}{4Is(Y + C_s s)}},
\end{aligned}
\tag{3}
$$

and s is the Laplace variable, $U(s)$ is the Laplace transform of the base excitation $u(t)$. By replacing z with L, we have the transfer function relating the tip displacement to the base displacement.

The governing PDE for charge density distribution $\rho(x,z,t)$ within IPMC is given by [37]

$$
\begin{aligned}
&\frac{\rho(x,z,t)}{\partial t} - d\frac{\partial^2 \rho(x,z,t)}{\partial x^2}\\
&\quad + \frac{F^2 dC^-}{\kappa_e RT}(1 - C^-\Delta V)\rho(x,z,t) = 0,
\end{aligned}
\tag{4}
$$

where F is Faraday's constant, R is the gas constant, T is the absolute temperature, ΔV is the volumetric change, d denotes the ionic diffusivity, C^- denotes the anion concentration, and κ_e denotes the effective dielectric constant of the polymer. Finally, with the base excitation $U(s)$ as input and the short-circuit current $I(s)$ as output, the transfer function for the complete sensing model is [29]

$$
\begin{aligned}
H(s) &= \frac{I(s)}{U(s)} = \frac{sQ(s)}{U(s)}\\
&= \frac{bYs(\beta(s)h\coth(\beta(s)h) - 1)}{\alpha_o \beta^2(s)}\frac{N_3(s)}{D_1(s)},
\end{aligned}
\tag{5}
$$

where α_o is the charge−stress coupling constant [37, 40], and

$$
\begin{aligned}
N_3(s) &= 2p[\cos(pL)\sinh(pL) - \cosh(pL)\sin(pL)],\\
\beta(s) &= \sqrt{\frac{s+K}{d}},\\
K &\triangleq \frac{F^2 dC^-}{\kappa_e RT}(1 - C^-\Delta V).
\end{aligned}
\tag{6}
$$

3 Experimental methods

The humidity-dependence of the IPMC sensor is characterized based on the identification of the humidity-dependent physical parameters of interest at different humidity levels. To create an environment with controlled humidity levels, a customized humidity chamber is built, where the humidity level inside is feedback-controlled by properly activating/deactivating a humidifier or dehumidifier. Under different humidity levels, the empirical frequency responses for the beam dynamics and the sensing output are obtained, and the static charging responses of the IPMC are collected. Then at each given humidity level, the physical parameters are acquired by curve-fitting the measured frequency response with the sensing model presented in Sect. 2, except for the effective dielectric constant κ_e, which is identified based on the effective capacitance of the IPMC under static charging.

3.1 Experimental setup

The schematic and the picture of the experimental setup are shown in Fig. 2a, b, respectively. The custom-built humidity chamber is made of acrylic sheets and well sealed. Inside this humidity chamber, one humidity sensor (HIH-4030, Honeywell) measures the relative humidity (RH) level and the data acquisition system (RTI 1104, dSPACE) collects its sensing result. When the measured humidity level deviates from the preset value consistently, the control circuit inside the chamber will receive a control signal from the dSPACE system and turn on/off the humidifier (EMS-200, Stadler Form) or the dehumidifier (EDV1100, Eva-Dry) accordingly. A temperature sensor is also used for monitoring purposes. Near the humidity sensor, an IPMC sample is clamped at one end on a rigid bar which goes through the chamber wall and is fixed on a mini-shaker (Type 4810, Brüel & Kjær). A flexible shaft cover printed by a 3D printer (Objet350 Connex, Stratasys Ltd.) is attached to the rigid bar, allowing the bar to vibrate freely while maintaining good sealing at the same time. Outside the humidity chamber, the mini-shaker excites the rigid bar with some controlled frequency and is mounted in such a way that the vibration direction is within the

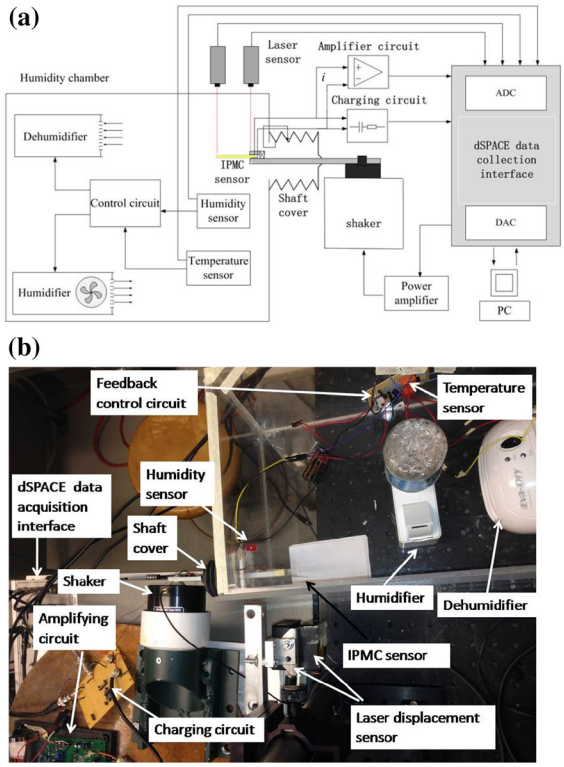

Fig. 2 The schematic (**a**) and photo (**b**) of the experimental setup

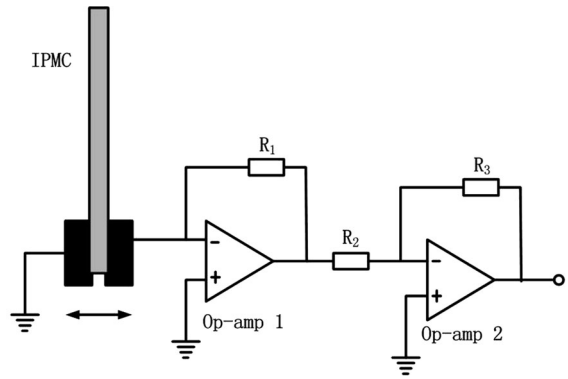

Fig. 3 Two-tier amplification circuit for measuring the short-circuit sensing current of the IPMC sensor

Table 1 Physical constants and directly measured parameters

F (C/mol)	R (J mol^{-1}K^{-1})	T (K)	L (mm)
96,487	8.3143	293	27.68
b (mm)	h (μm)		m (g/m)
5.26	130–150		3.48 – 3.68

horizontal plane. Two laser displacement sensors (OADM 20I6441/S14F, Baumer Electric) are mounted against the IPMC beam, measuring the base displacement and the tip displacement, respectively. The beam dynamics recorded by these two laser sensors allows us to identify the mechanical parameters separately. Note that the mounting frame for the laser sensors is isolated from the table where the mini-shaker is mounted. The signal conditioning module consists of a two-tier amplification circuit used to measure the short-circuit sensing current generated by the IPMC in the base-excitation experiments, a current sensor used to measure the charging current in the static charging experiments, and a switch circuit to switch the measurement between sensing current and charging current. Figure 3 shows the schematic of the two-tier amplification circuit, which consists of two cascaded operational amplifiers (op-amps). Op-amp 1 (OPA124, Texas Instruments Incorporated) is a low noise precision difet operational amplifier with high impedance. Since the inverting input of op-amp 1 is virtually the ground, the two electrodes of the IPMC sensor are short-circuited. Op-amp 2 is introduced for gain adjustment. In our experiment, we use $R_1 = 470\,\text{k}\Omega, R_2 = 10\,\text{k}\Omega$, and $R_3 = 20\,\text{k}\Omega$. Generation of control signal and vibration stimulus, acquisition of all the sensor output, and data processing are all performed through the dSPACE system. The IPMC sample used in this paper was originally purchased from Environmental Robots Inc. (Na^+ based). To reduce its surface resistance significantly, the sample was deposited with a layer of gold (0.2 µm thick) on each side in the e-beam physical vapor deposition system (Kurt Lesker AXXIS^{TM} PVD system).

Table 1 lists the physical constants and the parameters obtained through direct measurement. The temperature and the geometric dimensions are read directly from the temperature sensor and a digital caliper (Neiko 01407A), respectively. Note that there are two values for both the thickness and the mass per unit length. For each case, the first value was obtained by measuring the sample at 0 % RH level and the second one at 100 % RH level. Assuming that the change of the thickness and the mass per unit length is linear with the RH level, we use linearly humidity-dependent h and m for the rest of the paper to minimize

the influence of varying geometry and weight of the IPMC sensor caused by the different humidity levels. For the length L and width b, there are much less noticeable changes in their measurement, hence they are treated as constants in this paper.

3.2 Parameter identification

To investigate the IPMC sensing dynamics under different humidity levels, experiments for the base-excitation and the static charging are repeated at varying RH levels ranging from 38 to 80 %. The lower bound of RH levels is determined by the capability of the dehumidifier and the sealing of the humidity chamber, while the upper bound is determined by the measuring limitation of laser sensors (the chamber wall loses transparency under high RH levels). At each testing RH level, the IPMC sample is first base-excited under a sweep frequency ranging from 10 to 150 Hz, followed by switching off the circuit for the base-excitation experiment. After stabilization for 10 s, the circuit for the static charging experiment is switched on and the charging current of the IPMC is collected. By switching on/off the measurement circuit for sensing current or charging current, the electrical correlation between the two measurements is minimized. After a new testing RH level is set, the humidity sensor output needs to be monitored. Once the RH level becomes stable, it is ready for the experiments. This stabilization process usually takes 2–3 min. Then it takes 80 s to complete both of the experiments, during which the RH level inside the chamber is maintained constant. Due to the excellent sealing of the chamber, the maintained RH level throughout an experiment shows a maximum variability of $\pm 3\,\%$. The lower frequency bound is determined by the mini-shaker characteristics and the base-excitation configuration (sensing signal is weak under low frequency), while the upper bound is determined by the response time of the laser displacement sensors (close to 1 ms). Despite the experimental limitation, the test range of RH level and vibration frequency covers many applications that are of interest. The whole experimental setup is located in a well-maintained laboratory, where the temperature is kept at $20\,^{\circ}\mathrm{C}$. The monitoring output of the temperature sensor indicates a temperature variability less than $\pm 2\,^{\circ}\mathrm{C}$, therefore the temperature influence on the IPMC sensor performance is not considered in this study.

The Young's modulus Y, strain-rate damping coefficient C_s, and viscous air damping coefficient C_a are first identified by the empirical frequency response for the beam dynamics with the IPMC base displacement $u(t)$ as input and the tip displacement $w(L,t)$ as output, as shown in (2). Both $u(t)$ and $w(L,t)$ are measured by the laser sensors. To be specific, we fix an excitation frequency f and acquire $u(t)$ and $w(L,t)$. Fast Fourier transform (FFT) is performed on $u(t)$ and $w(L,t)$ to extract the amplitudes and phases of these two signals, which are then used to compute the magnitude gain and phase shift of the beam dynamics at that particular frequency. By repeating this process for other vibration frequencies, we obtains the empirical frequency response for the beam dynamics. Since the viscous air damping coefficient C_a is much smaller than Y and C_s, C_a is first assumed to be zero; then the two parameters Y and C_s are tuned by curve-fitting the frequency response of the mechanical dynamics using the Matlab function *fminsearch*. Next, the fitted values of Y and C_s are used as the initial values for a new run of curve-fitting which includes Y, C_s, and C_a together. By estimating the three mechanical parameters in this way, we can avoid local optimal solutions of *fminsearch*.

The effective dielectric constant κ_e is identified through the constant-voltage charging process, where a voltage of 0.1 V is used. Here IPMC is treated as a parallel-plate capacitor which contains the hydrated polymer that completely fills the space between the plates, and the capacitance is given by: $C_{cap} = \kappa_e \frac{WL}{2h}$ [41]. Therefore, κ_e can be calculated via $\kappa_e = C_{cap} \frac{2h}{WL}$ with $C_{cap} = \frac{Q_c}{U_c}$, where U_c is the fixed charging voltage and the accumulated charge Q_c is measured by integrating the charing current. We note that in reality, IPMC electrodes are not perfectly flat conducting plates, which implies that the aforementioned approach for measuring κ_e could introduce error. Considering (6), we can verify that the influence of κ_e on the overall model is limited when the diffusivity constant d is less than $10^{-13}\,\mathrm{m}^2/\mathrm{s}$, which is close to the maximum fitted value of d throughout the tested RH range in this work. In general, however, a more accurate method for determining κ_e is expected to result in improved prediction performance of the sensing model.

Once Y, C_s, C_a and κ_e are identified, they are plugged into the sensing model $H(s)$ for estimating the

remaining parameters (see below) using a similar curve-fitting strategy. Two experimental data are used together to identify the parameters, as shown in Fig. 4 for one result of curve-fitting under RH of 70 %. Similar results are observed under other testing RH levels. For the effective dielectric constant, the mean value of two experimental measurements is used (see Fig. 8). Note that the second experiment was repeated two days after the first experiment; however, no significant variability was found between these two experiments. Considering that the repeatability performance of an IPMC sensor in air is typically weakened by the changing temperature and humidity level in the ambient environment, it is expected to have consistent results between experiment 1 and experiment 2 in Fig. 4 where the data were collected at the same room temperature (20 °C) and the same humidity level.

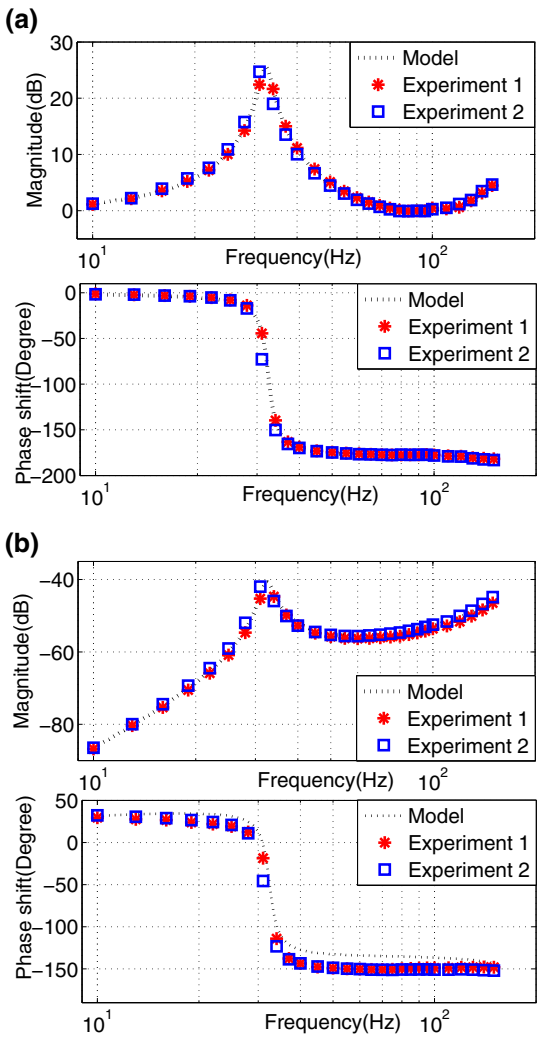

Fig. 4 Comparison of the measured frequency responses with model predictions (with identified parameters) under relative humidity of 70 % for: **a** beam dynamics (input: base excitation; output: tip displacement); **b** sensing dynamics (input: base excitation; output: IPMC short-circuit current)

4 Results and discussion

There are eight physical parameters in total in the sensing model $H(s)$, of which three (Y, C_s, and C_a) are from the beam dynamics in (1), four (ΔV, C^-, d, and κ_e) are from the charge dynamics in (4), and one (α_o) is from the assumption in [37, 40]. For those four parameters from the charge dynamics and the charge−stress coupling constant α_o, we only focus on the discussion on the ionic diffusivity d and the dielectric constant κ_e, both of which have explicit physical properties and have showed considerably large humidity-dependence in the experimental results. Since $|C^-\Delta V| \ll 1$ [37], we take $1 - C^-\Delta V \approx 1$, thus the volumetric change ΔV is ignored in the sensing model $H(s)$. Instead, the volumetric change is taken into account by using the linearly humidity-dependent h and m (see Table 1). The anion concentration and charge−stress coupling coefficient did not show clear dependence on humidity in our experiments and are thus treated as constants (94.64 J/C).

4.1 Humidity-dependent parameters

Figures 5, 6, 7, 8, 9 show the identified five physical parameters corresponding to a set of ten relative humidity levels (38 % and from 40 to 80 % with each increment of 5 %). By fitting the values of each parameter at different RH levels with the least-square method ("polyfit" function in Matlab), we obtain low-order polynomial functions of the RH (ranging from 38 to 80 %) for these five parameters. To be specific, Fig. 5 shows the identified Young's modulus Y at different relative humidity levels (denoted as ϕ_r), along with the approximating quadratic function

$$Y(\phi_r) = -2.134 \times 10^5 \phi_r^2 + 1.521 \times 10^7 \phi_r + 6.309 \times 10^8. \quad (7)$$

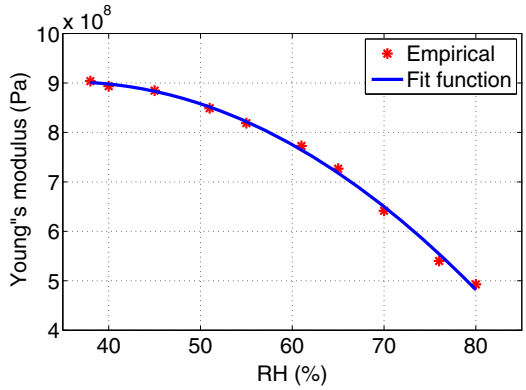

Fig. 5 Fitting function for Young's modulus Y

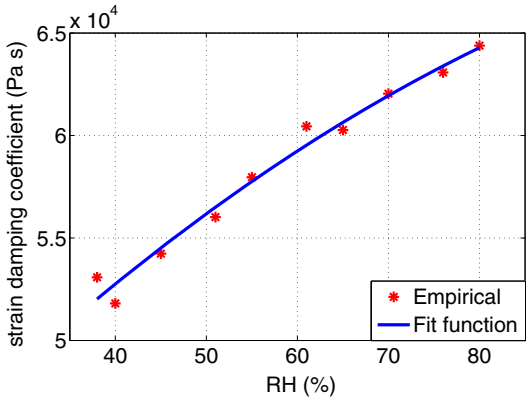

Fig. 6 Fitting function for strain-rate damping coefficient C_s

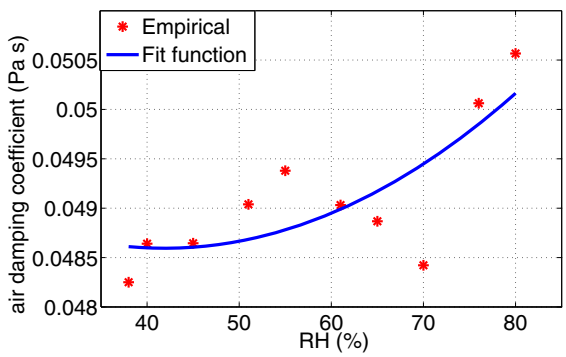

Fig. 7 Fitting function for viscous air damping coefficient C_a

Figure 6 shows the identified strain-rate damping coefficient C_s along with the approximation by the quadratic function

$$C_s(\phi_r) = -1.812\phi_r^2 + 5.057 \times 10^2 \phi_r + 3.542 \times 10^4. \tag{8}$$

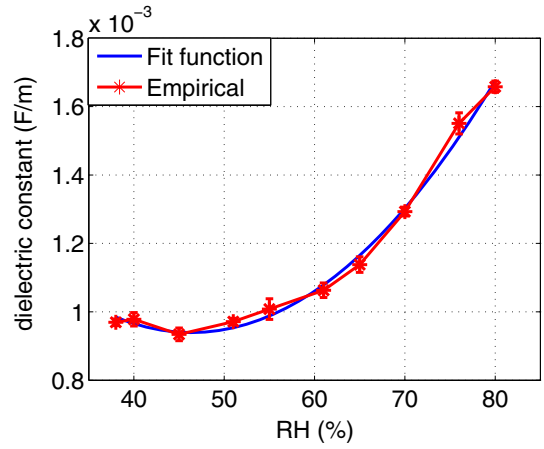

Fig. 8 Fitting function for dielectric constant *ke*

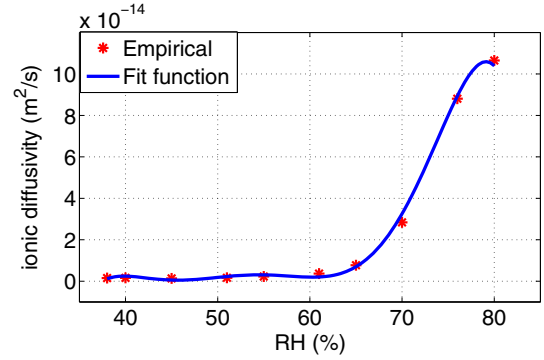

Fig. 9 Fitting function for ionic diffusivity d

Figure 7 shows the identified viscous air damping coefficient C_a along with the approximation by the quadratic function

$$C_a(\phi_r) = 1.080 \times 10^{-6}\phi_r^2 - 9.044 \times 10^{-5}\phi_r + 0.051. \tag{9}$$

Figure 8 shows the measured effective dielectric constant κ_e along with the approximation by the quadratic function

$$ke(\phi_r) = 6.499 \times 10^{-7}\phi_r^2 - 6.026 \times 10^{-5}\phi_r + 0.0023, \tag{10}$$

and Fig. 9 shows the estimated ionic diffusivity d along with the approximation by the six-order polynomial function

$$d(\phi_r) = -1.285 \times 10^{-21}\phi_r^6 + 4.307 \times 10^{-19}\phi_r^5 - 5.928 \times 10^{-17}\phi_r^4 + 4.291 \times 10^{-15}\phi_r^3 - 1.724 \times 10^{-13}\phi_r^2 + 3.645 \times 10^{-12}\phi_r - 3.1713 \times 10^{-11}. \quad (11)$$

Among three mechanical parameters (Y, C_s, C_a), the Young's modulus Y and the strain-rate damping coefficient C_s continuously decreases and increases, respectively, as the humidity level goes up. Based on the understanding of their physical characteristics, it is reasonable to have such observation for Y and C_s. Young's modulus is a measure of the material stiffness, and is expected to drop when the material becomes softer under increasing RH levels. Strain-rate damping accounts for the structural damping due to the internal energy dissipation of the beam. When the beam absorbs more water moisture into its polymer structure, the internal energy dissipation is expected to be faster, thus the damping coefficient C_s becomes larger. The air viscous damping coefficient C_a is also expected to increase with the RH level. While Fig. 7 shows that the identified C_a overall shows an increasing trend, the values between 60 and 70 % RH seem to be deviating from this trend. While the exact explanation for this phenomenon is still under investigation, we believe that the relatively weak contribution of the air viscous damping in the beam dynamics equation (1) reinforces the randomness of the identified C_a through curve-fitting with the non-ideal experimental conditions.

The effective dielectric constant κ_e is directly measured through the constant-voltage charging process, during which the IPMC sensor is treated as a parallel-plate capacitor containing the hydrated ionic polymer as the dielectric. Since the dielectric constant of water is larger than that of the ionic polymer, it is expected to see that κ_e continuously increases when the RH level goes up. Similarly, for ionic diffusivity d, it is straight forward to expect continual growth when the humidity level increases. The general trends of the identified parameters in Figs. 8 and 9 are consistent with these expectations. It can be seen in Fig. 9, d grows very slowly at the RH levels <60 %. Beyond this point, d starts to keep increasing quickly. Since the ionic diffusivity d varies in a relatively large range from the scale of 10^{-15} to 10^{-13}, a high-order polynomial function is used to approximate it. There are also other functions that can be used to fit the data in Fig. 9.

4.2 Validation of humidity-dependent model

To verify its prediction capability, we construct the humidity-dependent models for beam dynamics (2) and IPMC sensing (5) at the relative humidity of 68 % based on the humidity-dependent parameters of $Y(\phi_r), C_s(\phi_r), C_a(\phi_r), ke(\phi_r)$, and $d(\phi_r)$ evaluated at $\phi_r = 68$, respectively, based on (7), (8), (9), (10), and (11). Note that 68 % RH was chosen arbitrarily, but not used in data-fitting for approximating the polynomial functions. We have also constructed the similar models based on some fixed parameters, which were parameters identified under the RH level of 45 %. 45 % RH was also chosen arbitrarily and for comparison purpose only. These models are denoted as humidity-independent models. Figure 10 shows the comparison of beam dynamics between the measured frequency response and the two predicted frequency responses based on the humidity-dependent models and humidity-independent models, and Fig. 11 shows the comparison of sensing dynamics. It can be seen from both figures that good agreement is achieved both in magnitude gain and phase shift between the experimental measurement and the prediction of the humidity-dependent model, but the prediction of the

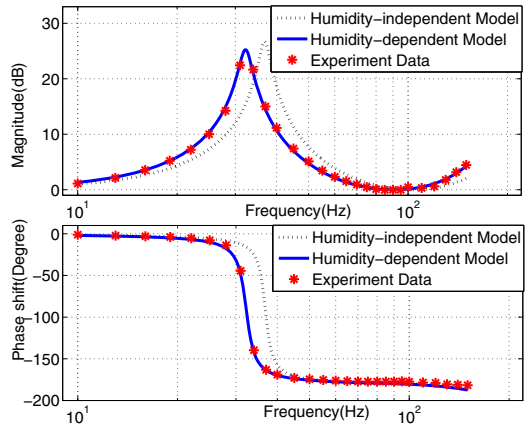

Fig. 10 Comparison of the measured frequency responses of beam dynamics with the two model predictions at the relative humidity of 68 %. The base displacement and the tip displacement are the input and output of the system, respectively

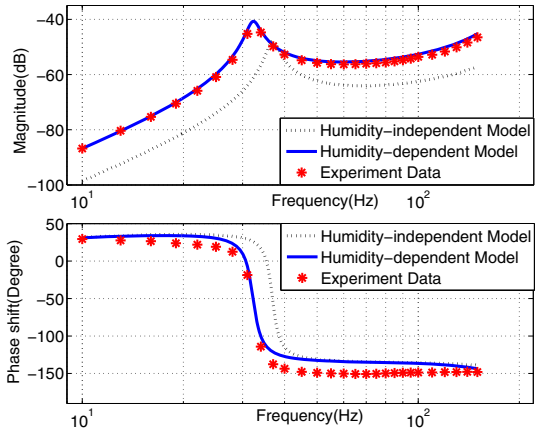

Fig. 11 Comparison of the measured frequency responses of sensing with the two model predictions at the relative humidity of 68 %. The base displacement and the short-circuit current are the input and output of the system, respectively

humidity-independent model shows large discrepancy from the measured frequency response, indicating that the proposed modeling approach is effective in capturing the humidity-dependent mechanical and sensing dynamics for IPMC.

5 Conclusion

In this study, we investigated the influence of humidity on IPMC sensing behavior from a physical perspective. We characterized and modeled the IPMC sensing dynamics by identifying the humidity-dependent physical parameters, including the Young's modulus, strain-rate damping coefficient, viscous air damping coefficient, effective dielectric constant, and ionic diffusivity. The empirical frequency responses of the sensor under different humidity levels were first obtained using a custom-built humidity chamber with controlled humidity levels, where the IPMC sensor was base-excited within the horizontal plane to minimize the gravity effect. The humidity-dependent physical parameters were then estimated by curve-fitting the measured frequency responses based on the proposed physics-based model. We also conducted charging experiments on the IPMC sensor and directly identified the effective dielectric constant. These parameters show a clear trend of change with the humidity. We further modeled the humidity-dependence of the physical parameters with polynomial functions, which were then plugged into the physics-based model to predict the sensing output under other humidity conditions. Experimental results have validated the humidity-dependent model.

Acknowledgments This work was supported in part by National Science Foundation (ECCS 0547131, DBI 0939454) and the Office of Naval Research (N000141210149).

References

1. Bar-Cohen Y (2004) Electroactive polymer (EAP) actuators as artificial muscles: reality, potential and challenges. SPIE Press, Bellingham, WA
2. Shahinpoor M, Kim KJ (2001) Ionic polymer–metal composites: I. Fundamentals. Smart Mater Struct 10:819
3. Kim KJ, Shahinpoor M (2003) Ionic polymer–metal composites: II. Manufacturing techniques. Smart Mater Struct 15:65
4. Lei H, Li W, Tan X (2012) In: Bar-Cohen Y (ed) Electroactive polymer actuators and devices (EAPAD) XIV, proceedings of SPIE, vol 8340. SPIE, Bellingham, WA, p 83401A
5. Shen L, Cha Y, Shams A, Porfiri M (2013) Fabrication and buckling analysis of ionic polymer metal composite pipes. Smart Mater Struct 22(10):105032
6. Chen Z, Tan X (2010) Monolithic fabrication of ionic polymer−metal composite actuators capable of complex deformation. Sens Actuators A Phys 157(2):246
7. Lei H, Tan X (2013) In: Bar-Cohen Y (ed) Electroactive polymer actuators and devices (EAPAD), proceedings of SPIE, vol 8687. SPIE, San Diego, CA, p 868707
8. Lei H, Li W, Tan X (2014) Encapsulation of ionic polymer–metal composite (IPMC) sensors with thick parylene: fabrication process and characterization results. Sens Actuators A Phys 217:1
9. Palmre V, Pugal D, Kim KJ, Leang KK, Asaka K, Aabloo A (2014) Nanothorn electrodes for ionic polymer–metal composite artificial muscles. Sci Rep 4:6176
10. Bauer F, Denneler S, Willert-Porada M (2005) Influence of temperature and humidity on the mechanical properties of Nafion 117 polymer electrolyte membrane. J Polym Sci B Polym Phys 43(7):786
11. Shoji E, Hirayama D (2007) Effects of humidity on the performance of ionic polymer–metal composite actuators: experimental study of the back-relaxation of actuators. J Phys Chem B 111(41):11915
12. Brunetto P, Fortuna L, Giannone P, Graziani S, Strazzeri S (2010) Static and dynamic characterization of the temperature and humidity influence on IPMC actuators. IEEE Trans Instrum Meas 59(4):893
13. Brunetto P, Fortuna L, Giannone P, Graziani S, Strazzeri S (2011) Characterization of the temperature and humidity influence on ionic polymer–metal composites as sensors. IEEE Trans Instrum Meas 60(8):2951
14. Ganley T, Hung DLS, Zhu G, Tan X (2011) Modeling and inverse compensation of temperature-dependent ionic

polymer–metal composite sensor dynamics. IEEE/ASME Trans Mechatron 16(1):80
15. Dong R, Tan X (2012) Modeling and open-loop control of IPMC actuators under changing ambient temperatures. Smart Mater Struct 21:065014
16. Park K (2011) Characterization of the solvent evaporation effect on ionic polymer−metal composite sensors. J Korean Phys Soc 59(6):3401
17. Aureli M, Porfiri M (2013) Nonlinear sensing of ionic polymer metal composites. Contin Mech Thermodyn 25(2–4):273
18. Lei H, Li W, Zhu G, Tan X (2012) Proceedings of ASME 2012 conference on smart materials, adaptive structures and intelligent systems, evaluation of encapsulated IPMC sensor based on thick parylene coating. ASME, Stone Mountain, GA, p 7975
19. Chen Z, Tan X, Will A, Ziel C (2007) A dynamic model for ionic polymer–metal composite sensors. Smart Mater Struct 16:1477
20. Cha Y, Aureli M, Porfiri M (2012) A physics-based model of the electrical impedance of ionic polymer metal composites. J Appl Phys 111(2):124901
21. Sun Z, Hao L, Chen W, Li Z, Liu L (2013) A novel discrete adaptive sliding-mode-like control method for ionic polymermetal composite manipulators. Smart Mater Struct 22(9):095027
22. Cha Y, Porfiri M (2013) A bias-dependent model of the electrical impedance of ionic polymer metal composites. Phys Rev E 87(2):022403
23. Aureli M, Porfiri M (2013) Nonlinear sensing of ionic polymer metal composites. Contin Mech Thermodyn 25(2):273
24. Cha Y, Porfiri M (2014) Mechanics and electrochemistry of ionic polymer metal composites. J Mech Phys Solids 71:156–178
25. Bonomo C, Fortuna L, Giannone P, Graziani S, Strazzeri S (2008) A resonant force sensor based on ionic polymer metal composites. Smart Mater Struct 17(1):015014
26. Bahramzadeh Y, Shahinpoor M (2011) Dynamic curvature sensing employing ionic-polymer–metal composite sensors. Smart Mater Struct 20(9):094011
27. Chen X, Zhu G, Yang X, Hung DL, Tan X (2013) Model-based estimation of flow characteristics using an ionic polymer–metal composite beam. IEEE/ASME Trans Mechatron 18(3):932
28. Zangrilli U, Weiland LM (2011) Prediction of the ionic polymer transducer sensing of shear loading. Smart Mater Struct 20(9):094013
29. Lei H, Lim C, Tan X (2013) Modeling and inverse compensation of dynamics of base-excited ionic polymermetal composite sensors. J Intell Mater Syst Struct 24(13):1557
30. Cellini F, Intartaglia C, Soria L, Porfiri M (2014) Effect of hydrodynamic interaction on energy harvesting in arrays of ionic polymer metal composites vibrating in a viscous fluid. Smart Mater Struct 23(4):045015
31. Cha Y, Verotti M, Walcott H, Peterson SD, Porfiri M (2013) Energy harvesting from the tail beating of a carangiform swimmer using ionic polymer metal composites. Bioinspir Biomim 8(3):036003
32. Cha Y, Shen L, Porfiri M (2013) Energy harvesting from underwater torsional vibrations of a patterned ionic polymer metal composite. Smart Mater Struct 22(5):055027
33. Peterson SD, Porfiri M (2012) Energy exchange between a vortex ring and an ionic polymer metal composite. Appl Phys Lett 100(11):114102
34. Lim C, Lei H, Tan X (2013) In: Bar-Cohen Y (ed) Electroactive polymer actuators and devices (EAPAD) XIV, proceedings of SPIE, characterization and modeling of humidity-dependence of ipmc sensing dynamics, vol 8687. SPIE, Bellingham, WA, p 868720
35. Lim C, Lei H, Tan X (2012) In: Bar-Cohen Y (ed) Electroactive polymer actuators and devices (EAPAD) XIV, proceedings of SPIE, a dynamic, physics-based model for base-excited IPMC sensors, vol 8340. SPIE, Bellingham, WA, p 83400H
36. Aureli M, Prince C, Porfiri M, Peterson SD (2010) Energy harvesting from base excitation of ionic polymer metal composites in fluid environments. Smart Mater Struct 19(1):015003
37. Nemat-Nasser S, Li J (2000) Electromechanical response of ionic polymer–metal composites. J Appl Phys 87(7):3321
38. Clough RW, Penzien J (1975) Dynamics of structures. McGraw-Hill, New York
39. Erturk A, Inman DJ (2011) Piezoelectric energy harvesting, 1st edn. Wiley, London
40. Farinholt K, Leo DJ (2004) Modeling of electromechanical charge sensing in ionic polymer transducers. Mech Mater 36:421
41. Chen Z, Tan X (2008) A control-oriented and physics-based model for ionic polymer–metal composite actuators. IEEE/ASME Trans Mechatron 13(5):519